Received: 5 January 2024 | Revised: 21 February 2024 | Accepted: 27 February 2024

DOI: 10.1002/pen.26698

RESEARCH ARTICLE

POLYMER ENGINEERING AND SCIENCE WILEY

Relation of craze to crack length during slow crack growth phenomena in high-density polyethylene

Markus Schilling | **Ute Niebergall** | **Niklas Marschall** | **Dietmar Meinel** | **Martin Böhning**

Bundesanstalt für Materialforschung und –prüfung (BAM), Berlin, Germany

Correspondence
Martin Böhning, Bundesanstalt für Materialforschung und –prüfung (BAM), Unter den Eichen 87, 12205 Berlin, Germany.
Email: martin.boehning@bam.de

Funding information
AiF Arbeitsgemeinschaft industrieller Forschungsvereinigungen "Otto von Guericke" e.V. / German Federation of Industrial Research Associations

Abstract

The craze-crack mechanism occurring in high-density polyethylene (HDPE) causing slow crack growth and environmental stress cracking is investigated in detail with respect to the relation of crack length and the related craze zone. This is essential for the understanding of the resulting features of the formed fracture surface and their interpretation in the context of the transition from crack propagation to ductile shear deformation. It turns out that an already formed craze zone does not inevitably result in formation of a propagating crack, but could also undergo ductile failure. For the examination, the full notch creep test (FNCT) was employed with a subsequent advanced fracture surface analysis that was performed using various imaging techniques: light microscopy, laser scanning microscopy, scanning electron microscopy, and X-ray micro computed tomography scan. FNCT specimens were progressively damaged for increasing durations under standard test conditions applying Arkopal, the standard surfactant solution, and biodiesel as test media were used to analyze the stepwise growth of cracks and crazes. From considerations based on well-established fracture mechanics approaches, a theoretical correlation between the length of the actual crack and the length of the preceding craze zone was established that could be evidenced and affirmed by FNCT fracture surface analysis. Moreover, the yield strength of a HDPE material exposed to a certain medium as detected by a classic tensile test was found to be the crucial value of true stress to induce the transition from crack propagation due to the craze-crack mechanism to shear deformation during FNCT measurements.

Highlights

- Progress of crack formation in high-density polyethylene is analyzed by different imaging techniques
- Determined growth rates depend on distinction between craze zone and crack

- The ratio of the present crack to the anteceding craze zone is validated theoretically
- The transition from crack propagation to ductile shear deformation is identified
- An already formed craze zone may still fail by ductile mechanisms

KEYWORDS

craze-crack mechanism, environmental stress cracking (ESC), full notch creep test (FNCT), laser scanning microscopy (LSM), slow crack growth (SCG), X-ray computed tomography (CT)

1 | INTRODUCTION

Since slow crack growth (SCG) and environmental stress cracking (ESC) as damage mechanisms must be considered the major causes of failure in application of polyolefins,[1,2] their detailed understanding is relevant for the development of resilient polyolefin materials. SCG and the related ESC, which can be regarded as slow crack growth accelerated by contact with certain liquid media, especially affect high-density polyethylene (HDPE). This is widely used as pipe material but also in other high-performance applications, such as material for jerrycans, drums, and intermediate bulk containers (IBC) for transport and storage of dangerous goods.[3] The possible contact with a wide range of fluids in those areas makes the resistance against ESC an essential issue. Generally, the failure of HDPE due to SCG/ESC is based on the propagation of a growing crack in the polymer material perpendicular to a mechanical load. During SCG/ESC mechanisms,[4] at first small voids emerge due to a local stress concentration caused by inhomogeneities, surface scratches, or defects in the material. These voids grow and coalesce and thereby, the material between the voids forms fibrillar structures, denoted as crazes, which elongate and finally break. Thus, the crazes turn into a crack, propagating as a result of a moving front of stress concentration leading to further voiding and crazing. Consequently, there is a craze zone and a crack that are propagating through the material leading finally to the ultimate failure of the entire part. This is denoted as the typical "craze-crack mechanism." Respective sizes of craze zone and crack and especially their length ratio during the damage process as well as their relation to the final failure are not entirely understood, so far. Regions in HDPE components that underwent crazing might be considered (pre)-damaged to some extent as their structure has obviously been changed by a commencing craze-crack mechanism. At least, the structure and properties of crazed regions are different to the original structure leading to a different behavior of the material under further stress. At first glance, the appearance of such crazes might be considered an indicator for an inevitable subsequent occurrence of cracks.

In this context it must be noted that due to a propagating crack also the effective residual cross-sectional area, which determines the actual stress due to a certain external mechanical load, is usually reduced. Hence, the actual stress increases continuously in the course of the crack propagation. This crack propagation due to SCG/ESC based on the craze-crack-mechanism occurs at stresses distinctly below the yield stress of the polyethylene material; at higher stress levels, a transition to ductile shear deformation takes place. Therefore, a reduction of the effective cross-sectional area due to crack propagation leads to significantly higher stress and thus, at a certain point, to a finally ductile failure of the material. This so-called brittle-ductile transition is well known for HDPE and a relation to the yield stress is likely.[5–8] The designation as "brittle" for the craze-crack mechanism arises from the rather flat and brittle appearance of the resulting fracture surface compared to the surface resulting from ductile tensile shear deformation.

This may result in the question, whether an already formed craze zone also inevitably fails by crack growth or if also an overall ductile behavior of this pre-damaged region is possible when the threshold stress is exceeded. This aspect is especially important for the test methods employing notched specimens where a post-failure analysis of the fracture surface provides valuable information about the damage progression and the underlying mechanisms.[3,5,6,8,9]

In this study, the full notch creep test (FNCT) is used to induce the classic craze-crack mechanism leading to failure by SCG/ESC. This method to test HDPE materials with respect to their resistance against SCG/ESC is widely applied (especially in Europe).[10,11] In the FNCT, a specimen with a circumferential notch is subjected to a constant static load immersed in a temperature-controlled environment that usually

contains a surface-active liquid. According to the FNCT standard ISO 16770,[7] size and geometry of the specimen (see also Section 3.3) are such that plane strain conditions (cf. Section 2) are obtained and predominantly brittle fracture occurs after a certain exposure time under appropriate conditions such as tensile load and temperature. The applied tensile load value is typically well below the yield stress of the tested material. It has to be chosen to ensure crack propagation to dominate the failure behavior, that is, to shift the unavoidable transition to ductile behavior to the latest stages of the test.[7,9] Furthermore, to realize test durations within practically acceptable timescales as well as to focus on craze-crack propagation, for the FNCT, a well-defined notch is applied in the test specimen for crack initiation. The determined time to failure, that is, breakage of the notched specimen, is usually taken as a measure for the resistance against SCG and ESC, respectively, depending on the medium in which the specimens were immersed.[3,12] ISO 16770[7] specifies an aqueous solution of a surfactant (e.g., Arkopal N100) as liquid environment, but other chemicals, such as air or distilled water, may be used as well. As it is known, surfactant solutions or other surface-active liquids accelerate the test (reduce time to failure values) compared to a test in water due to their influence on the craze-crack mechanism.[12]

For more detailed investigations of FNCT specimens failed or damaged as a result of the craze-crack mechanism, several imaging techniques such as light microscopy (LM), laser scanning microscopy (LSM), scanning electron microscopy (SEM), and X-ray micro computed tomography scan (CT) were used in a previous study.[3] This image-based fracture surface analysis of FNCT specimens has proven to be a valuable tool for the examination of underlying damage mechanisms and associated material behavior.[8,12] Using a series of partially damaged specimens, these techniques were able to provide effective crack propagation rates. However, in this previous study,[3] deviations in apparent crack growth rates obtained from destructive optical techniques (e.g., LM and LSM) compared to nondestructive imaging methods (e.g., scanning acoustic microscopy—SAM and CT) were found. These could only partly be ascribed to obvious differences in detection capabilities of the imaging techniques involved with respect to the distinction of craze and crack zones. This differentiation is due to different reflective properties originating from different sub-micrometer surface structures. But as these method-related effects did not completely account for the observed deviations, it was further assumed that the length of the craze zone increases with the continuously increasing crack length. This also leads to the question whether a formed craze zone also inevitably results in a brittle crack and therefore gives reason to reexamining and extending these experiments. A more detailed consideration of the conditions in terms of formed crazes and resulting cracks as well as fracture mechanics is sought in the present study. Furthermore, results for a second liquid medium are included for comparison and verification.

For the analysis and subsequent comparison of craze-crack growth and propagation rates induced by different test liquids, a series of partially damaged samples was prepared. For the nondestructive imaging techniques (such as CT), a typical single FNCT procedure was performed, but loading was interrupted intendedly multiple times before failure allowing for an analysis of the specimen after distinctly chosen time periods. Hence, several damage stages were analyzed using the same specimen. For those imaging techniques, in which the fracture surface has to be dissected (i.e., LM and LSM), multiple specimens were prepared by individual FNCT experiments which were aborted after the respective time periods. The fracture surfaces were then uncovered by cryo-fracture of the specimens in liquid nitrogen.[3] All samples were investigated with respect to length of craze zone and crack. This enables the identification of interdependencies and relations of craze zone and crack lengths and consider them theoretically based on classic fracture mechanics.

2 | THEORY OF FRACTURE MECHANICS WITH RESPECT TO CRAZE-CRACK BEHAVIOR

A deeper comprehension of the mechanisms governing SCG phenomena in HDPE can be achieved by delving into the realm of fracture mechanics. In this context, a more nuanced exploration was established by analyzing the brittle fracture behavior of glasses, pioneered by Griffith in the early 20th century.[13] This fracture theory also introduces the approach of linear elastic fracture mechanics (LEFM) into fracture analyses across diverse materials. It is universally applicable for fracture scenarios involving plastic deformations localized at a crack tip that do not incite overall yielding throughout the material.

In accordance with this theory, the process of fracture is anticipated to result in increased surface area within a specimen. Consequently, the hypothesis is that the energy needed to generate this additional surface area must be counterbalanced by a corresponding reduction of the energy fraction elastically stored. Moreover, it is suggested that this elastic energy is not evenly dispersed throughout the specimen; instead, it is supposed to be concentrated in proximity to minor cracks. This implies that fracture arises due to the propagation of cracks that initiate from localized defects.

The Irwin model further contributes to the understanding of crack propagation within the framework of fracture mechanics. This model connects the process of crack propagation to the stress field surrounding an idealized crack length, denoted as 2c.[14] Thus, crack propagation becomes directly linked to the applied stresses. In this model, the stress fields around the region of the crack maintain a consistent shape for different load situations perpendicular to the crack. The stress intensity for a given load and geometry is defined by the constant K_I, known as the "stress intensity factor," where the superscript "I" signifies a loading condition perpendicular with respect to the crack. Considering an infinite sheet with a central crack of the length 2c and with a uniform stress σ applied, the relationship for K_I is expressed as:

$$K_I = \sigma(\pi c)^{1/2.} \tag{1}$$

As soon as the external stress σ approaches the fracture stress σ_B, the stress intensity factor K_I approximates a critical value when,

$$K_{IC} = \sigma_B(\pi c)^{1/2.} \tag{2}$$

This critical stress intensity factor, K_{IC}, characterizes the stress field at the point of fracture.

Taking cues from the approach of Griffith and utilizing the definition of fracture stress, Equation (2) may be reformulated as:

$$\sigma_B = \left(\frac{{K_{IC}}^2}{\pi c}\right)^{\frac{1}{2}}. \tag{3}$$

Given the significant deviations between theoretical and experimental values for surface energies, a suggestion arose to incorporate an additional term into the surface energy equation that accounts for plastic deformation work during crack propagation.[15–17] This line of thought led to the development of the concept of describing polymer fracture in terms of a surface work parameter J. This parameter should be differentiated from the true surface energy. Additionally, Andrews introduced a comprehensive theory of fracture that considers a combination of viscoelastic and plastic deformation.[18] This theory concludes that, for polymers, the predominant contribution to surface energy arises from a process of viscous flow, linked to structures on the fracture surface termed "interference bands." The polymer chain alignment in front of a crack demands energy expenditure, leaving a layer of highly oriented fibrillar polymeric material in the wake of crack progression. Within this context, a tiny wedge of porous material forms at the crack tip, known as a "craze." Such a craze is established under conditions of plane strain, where lateral contraction of the polymer is restricted, leading to reduced density due to void formation.[19–21] The craze profile observed in polymer materials closely resembles the plastic zone model for metals of Dugdale.[22] Given that stress cannot become infinitely concentrated at a crack tip for practical reasons, two potential outcomes emerge: (1) For conditions of plane stress in thin materials or plane strain in thick sheets, a zone of shear yielding could manifest. (2) For conditions of plane strain in thick sheets, the singularity with respect to stress at the tip of the crack can be relieved through craze formation. In contrast to the oval (plane stress) or kidney-shaped (plane strain) shear yield zones, this results in a linear zone.[22] A constant craze stress σ_c is hypothesized, distinct from and likely lower than the yield stress (Figure 1). Due to the inherent differences between crazing and shear yielding, they exhibit distinct responses to alterations in polymer structure.

Building on Dugdale's plastic zone model (Figure 1), the length of the corresponding craze can be derived for a crack under propagation at a given point[23]:

$$s_{\text{craze}} = \frac{\pi}{8}\frac{K_{IC}^2}{\sigma_c^2} \tag{4}$$

where s_{craze} denotes the length of the craze zone, σ_c represents the craze stress, and K_{IC} is the critical stress intensity factor.

This approach facilitates a clearer grasp of the shift between brittle and ductile behaviors in polymers, considering the interplay between crazing and yielding. These processes are both based on activated mechanisms, responding differently to variations in temperature and strain rate. Depending on the specific external conditions, one of these processes may dominate during fracture. Within the plane, as a crack progresses, it traverses a line

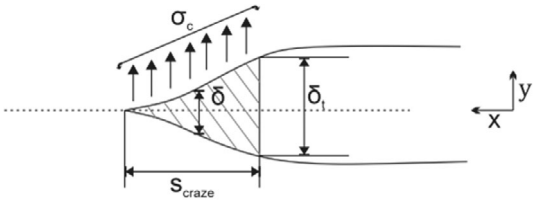

FIGURE 1 Dugdale plastic zone model for a craze (according to Dugdale[22]); σ_c: craze stress, s_{craze}: length of craze zone, δ: separation distance between upper and lower craze surface, δ_i: crack opening displacement (COD).

of shear stress zero but at the same time a triaxial stress at maximum. Such stress distributions promote craze formation with the extent of the corresponding craze being determined solely by the need to counterbalance the stress singularity at the tip of the crack (Equation 4).

To effectively investigate SCG/ESC rooted in craze-crack propagation, it is essential that extensive yielding (ductile shear deformation) does not influence the failure mechanisms. This prerequisite for credible evaluation of corresponding tests necessitates a brittle fracture appearance.[8,9] Practically, such brittle fracture behavior is observed under conditions of plane strain, achieved through either minimum specimen thickness or within localized specimen regions. Tailored testing methods such as the full notch creep test (FNCT) enable the creation of suitable conditions, aligning with a particular temperature and medium by selecting optimal specimen geometry and load levels. This also makes the consideration of the J-integral approach abdicable.[24–28]

3 | MATERIALS AND MEDIA

3.1 | High-density polyethylene material

A common and commercially available PE resin (HDPE type) was chosen for our investigation, exhibiting unimodal molecular weight distribution: Lupolen 4261 AGUV 60005, referred to as "AGUV" in the following. As this material is especially designed for high-performance applications, it is of great practical relevance in the field of container applications for transport and packaging of dangerous goods, such as fuels (jerrycans, IBC). AGUV has a density of 0.945 g/cm^3 and a melt flow rate (MFR, 190°C, 21.6 kg) of 6 g/(10 min). Further characteristic properties are a melting temperature of 130°C and a tensile modulus of 850 MPa at 23°C (data taken from data sheets[29] of LyondellBasell (Basell Polyolefine GmbH, Frankfurt/Main, Germany), who also kindly provided the HDPE material). Furthermore, AGUV contains special stabilizers to be particularly protected against heat and UV-radiation.

3.2 | Media

Following ISO 16770,[7] FNCT tests were performed in a 2 wt% aqueous solution of the surfactant Arkopal N100 (4-nonylphenyl-polyethylene glycol, 680 g/mol avg. molecular weight) at 50°C (cf.[8]). Arkopal N100 was kindly provided by Clariant GmbH, Frankfurt/Main, Germany. For this study, FNCT experiments were additionally performed in biodiesel. Biodiesel was obtained from ASG (ASG Analytik-Service Gesellschaft mbH, Neusäß, Germany) providing pure biodiesel from rapeseed methyl ester (RME) without additives (EN 14214[30]). Due to observed strong differences in the time to failure t_f between FNCT experiments performed in Arkopal and biodiesel,[12] different characteristics of the craze-crack mechanism could be expected. Furthermore, biodiesel is significantly absorbed by HDPE, whereas the overall solubility of aqueous Arkopal solution in HDPE is almost negligible.[31]

3.3 | Sample preparation

All specimens (type B in ISO 16770[7]) with dimensions of (90 × 6 × 6) mm^3 used for FNCT experiments and subsequent imaging analysis were cut from sheets of 6 mm thickness. These were prepared in a heating press under conditions following ISO 293[32] and ISO 17855,[33] that is, processed for 5 minutes at a press temperature of 180°C and a pressure of 10 MPa. Cooling was performed subsequently at 15 K/min, the pressed sheets were removed below a press temperature of 40°C and then tempered at 100°C for 3 h. After cutting, FNCT specimens were notched circumferentially (depth 1 mm) using a semiautomatic device, which meets the requirements of ISO 16770,[7] ISO 13274,[34] and ISO 11542[35] (cf. Figure 2).

4 | EXPERIMENTAL SECTION

4.1 | FNCT procedure

In order to conduct standard FNCT measurements and prepare samples for subsequent fracture surface analysis (as discussed in Section 1), an FNCT device of IPT Institut für Prüftechnik Gerätebau, Todtenweis (Germany) was utilized. Beyond measuring the time to failure t_f, this device was equipped to continuously monitor and record the time-dependent elongation of the specimen. Each individual specimen was securely held between two removable clamps attached to a fixed jig (providing connection to the loading system and stress gauge as well as containing a temperature sensor) which was immersed in a dedicated stainless-steel vessel containing the liquid test medium[31] (either Arkopal or biodiesel), which was continuously stirred. A mechanical load, maintained at a constant force, was applied and maintained using a stepping motor in conjunction with a stress gauge. The temperature within the medium, proximal to the specimen, was measured and regulated via a heating plate positioned beneath the test cylinder. Further details about the FNCT device can be found in Schilling et al. (2017)[8,12], and Schilling (2020).[31]

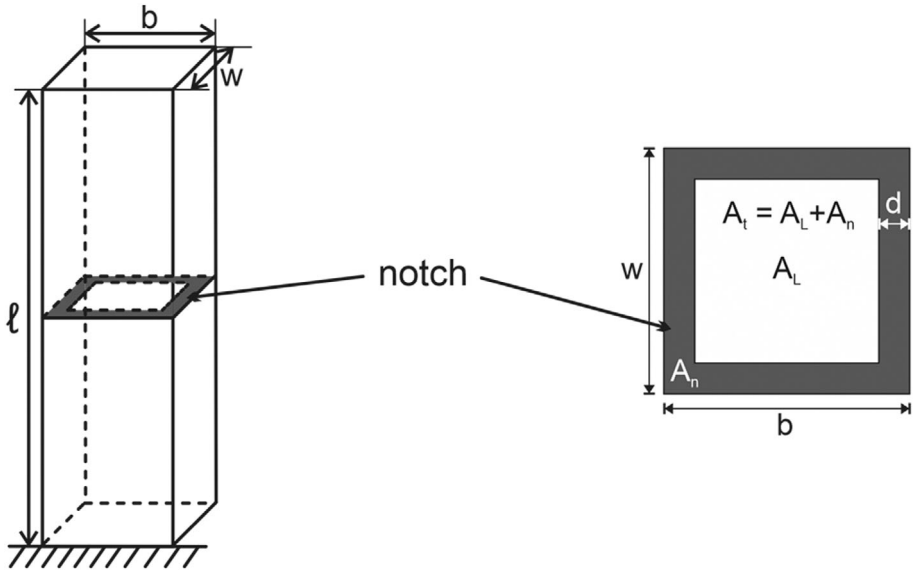

FIGURE 2 Specimen geometry for full notch creep test ($\ell = 90$ mm, $w = b = 6$ mm); sketch of the initial residual cross section (initial ligament area A_L) after applying the notch ($d = 1$ mm), area A_n of the notch resulting from notch depth d and the total cross-sectional area A_t.

Given that the jig holding the specimen needed to be in a defined state of tension at the start of measurement, an initial preloading step was essential. Consequently, a preload of 30 N was gradually applied at 1 N/s immediately after mounting an FNCT specimen into the device and immersing it in the test medium. This procedure ensured a consistent, reproducible, and well-defined starting point for all tests. Considering that typical forces applied ranged from 140 to 150 N (aligned with actual specimen dimensions and corresponding to a nominal stress of 9 MPa, as specified for HDPE container applications in ISO 16770[7]), this approach established an appropriate and sufficiently low stress level. The elongation measurement promptly commenced following preloading. Moreover, the experimental protocol encompassed the conditioning of clamped specimens within the temperature-controlled immersion medium for 10 hours prior to loading.

The standard FNCT procedure, as outlined in ISO 16770, involves determining the characteristic time to failure t_f^* for a specific combination of material and medium. This determination is supposed to be based on five individual measurements carried out at a temperature of 50°C, with load levels slightly varied above and below the nominal stress (referred to as the "reference stress") of 9 MPa. These load levels were set at 8.25, 8.75, 9.00, 9.25, and 9.75 MPa. The time to failure values obtained from each individual measurement were denoted as t_f. Following each test, that is, subsequent to specimen failure, the notch depth and the resultant actual initial residual cross-sectional area (referred to as the "ligament area" A_L after notching, as depicted in Figure 2) were meticulously measured using LM on the final fracture surfaces. This measurement allows for the calculation of the precise actual initial stress σ_L for each individual specimen, as described in Equation (5).

$$\sigma_L = \frac{F}{A_L}. \tag{5}$$

Especially with respect to σ_L, t_f^* is obtained accurately by a linear interpolation to the nominal stress of 9 MPa in the plot of the logarithmic time to failure values t_f of individual tests versus logarithmic values of the actual σ_L (see also[3,8]). This procedure was performed first and from the obtained t_f^*, the time steps for the partially damaged samples were determined on a percentage basis (Table 1).

For the analysis and subsequent comparison of craze-crack growth and propagation rates resulting from the occurring craze-crack mechanism induced by the different media used (Arkopal, biodiesel), partially damaged samples were prepared at nominal stresses of 9 MPa and 50°C. For this purpose, the test procedure similar to a single FNCT measurement was performed, but after distinctly chosen periods of time, loading was aborted and specimens were removed and analyzed. For the nondestructive CT experiments, all steps were performed intermittently on one single specimen, whereas for the destructive microscopy (LM and LSM), individual specimens were prepared and fractured by manual hammer impact in liquid nitrogen to uncover the fracture surface for analysis.

4.2 | Imaging analysis

In this study, fracture surfaces of broken FNCT specimens were subject to analysis using different imaging techniques. The analysis encompassed the use of techniques of optical

imaging such as LM and LSM which are destructive, that is, they require the dissection of the specimen in order to make the fracture surface accessible. The distinctive shapes and features of cryo-fractured regions and those arising directly from crack growth during FNCT exposure allowed for clear differentiation on the fracture surface, as evidenced in previous studies.[3] This differentiation played a pivotal role in the analysis process.

Moreover, intact FNCT specimens underwent scrutiny using the nondestructive imaging technique X-ray computed tomography scan. Additionally, SEM was harnessed to meticulously evaluate distinctive fracture surface features specific to FNCT.

For accurate crack length measurement and comparison, and to evaluate data displaying crack propagation derived from the various imaging techniques, an average crack length served as a crucial metric. To arrive at this average crack length, the initial step involved quantifying the measurements of damaged (cracked) and undamaged areas. These measurements were subsequently related to an idealized and normalized square area. Using this normalized framework, the average crack length was computed utilizing Equation (7), as visually depicted in Figure 3.

The formal definition of the average crack length c, related to real geometric proportions, is expressed as follows:

$$c = \bar{c} = \frac{\sum_{i}^{n} C_i}{n}. \tag{6}$$

This average crack length can also be deduced from the proportion between the damaged and undamaged areas, following the relationship illustrated schematically in Figure 3:

$$c = l - u = \frac{1}{2}\left(\sqrt{A_{fs}} - \sqrt{A_{ud}}\right). \tag{7}$$

Practically, the partial area A_{ud} (undamaged) and the total fracture surface A_{fs} are measured optically (e.g., from the LSM grayscale image exemplified in Figure 4A). The damaged area A_d is the difference between the two. According to the sketch in Figure 3 and Equation (7), the average crack length is calculated based on these areas A_{fs} and A_{ud}.

TABLE 1 Overall time to failure t_f^* percentages and exposure times for analysis by fracture surface imaging of all AGUV-medium systems applied in this study, respectively.

Percentage of t_f^*/%	Exposure time of AGUV, Arkopal/h	Exposure time of AGUV, biodiesel/h
0.0*,CT	0.00*	0.00*
0.2	0.10	0.02
1.0	0.60	0.10
2.0	1.10	0.20
5.0	2.80	0.50
15.0	8.50	1.50
25.0	14.20	2.50
33.0CT	18.70	3.30
40.0	22.60	4.00
50.0	28.30	5.00
60.0	34.00	6.00
66.0CT	37.40	6.60
75.0	42.50	7.50
85.0	48.10	8.50
97.0CT	54.90	9.70
98.5	55.80	9.85
100.0	56.60	10.00

Abbreviation: CT, CT measurements were performed only after these times of loading.
*Sample only notched, no loading/exposure.

4.2.1 | Light microscopy (LM), laser scanning microscopy (LSM), and scanning electron microscopy (SEM)

In order to accurately determine the actual initial stress related to the force applied to each individual specimen,

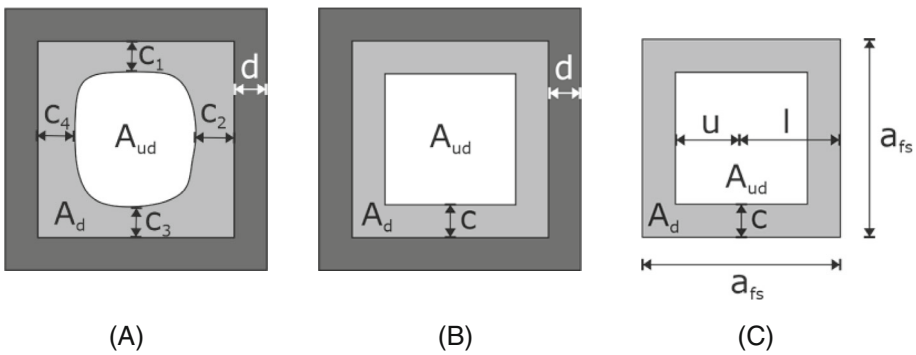

FIGURE 3 Projection and normalization of real surface area to calculate an average crack length (schematically depicted)[3]; A_d: damaged area, A_{ud}: undamaged area, c_1 ...c_4: real arbitrary crack lengths, c: average crack length, d: notch depth, a_{fs}: dimension of residual fracture surface (idealized square with total area of the fracture surface A_{fs}).

conventional optical LM employing a Zeiss AxioCam ICc 3 mounted on a Stemi 2000-C microscope was used. This method facilitated the measurement of the initial residual cross-sectional area of each test piece subsequent to notching. The overall time to failure t_f^*, associated with the nominal stress, was then determined through interpolation utilizing the individual t_f values (as elaborated in Section 4.1). Additionally, light microscopy enabled the initial analysis of fracture surfaces post-failure, providing insights into factors such as damaged and undamaged areas in partially damaged samples. These could be used in principle for the calculation of average crack lengths, as expounded in Section 4.2 through the utilization of Equation (7).

A more in-depth analysis was achieved through the utilization of LSM to meticulously examine FNCT fracture surfaces. For this purpose, a Keyence VK-X 100 instrument (Keyence GmbH, Neu-Isenburg, Germany) was used, featuring a semiconductor laser of 658 nm wavelength. Beyond offering detailed height information, LSM produced high-contrast achromatic laser images with a range of 65,536 gray shades. The LSM scanning process provided a 5 nm height resolution and employed a window size of 1407 × 1343 pixels. To encompass a wider range of overall height, multiple scans were conducted, incrementing the height by 12 µm for each scan. Notably, the grayscale laser images procured from the LSM exhibited better contrast, which led to their preference over images acquired via light microscopy. This contrast proved invaluable for distinguishing between regions damaged due to crack growth and those affected by subsequent manual cryo-breakage following FNCT exposure, a process pivotal for preparing partially damaged specimens. Figure 4 provides an illustrative example of this distinction.

The detailed quantitative 3D height information yielded by the LSM could be seamlessly imported into the Origin software (OriginLab Corporation, Northampton, MA, USA) for data analysis and graphical representation. This integration included an appropriate scaling of the height data along the z-axis, a step critical for ensuring a precise representation aligned with the plane of the notch as the zero-level reference. Adjustments were made by shifting the data points, achieved through the subtraction of the average height value of the circumferential notch area A_n which provided the reference point delineated in Figures 2 and 4. Subsequently, pixel-based data underwent transformation into metric values, followed by gridding using the Renka–Cline interpolation method[36] (as implemented in Origin), and plotted as a 3D surface image as exemplary depicted in Figure 5. These height profiles can be used for evaluation and assessment of FNCT fracture surfaces as demonstrated in Schilling et al. (2018), Schilling, Niebergall, Böhning (2017), and Schilling et al. (2021).[3,8,9] Nevertheless, for the quantitative evaluation of fracture surfaces in order to obtain crack propagation rates, the LSM grayscale images proved to be more suitable than the elaborate height profiles.

In pursuit of an even more comprehensive understanding of surface structure, an EVO MA10 SEM, engineered by Carl Zeiss Microscopy GmbH (Jena, Germany), was used. To prepare the specimens for SEM analysis, a sputter coater SCD 050 from Leica Microsystems (formerly Bal-Tec Balzers, Wetzlar, Germany) was utilized to deposit a gold layer. The process involved sputtering at 40 mA current for 100 s at room temperature, yielding a gold layer of approximately 25 nm thickness. SEM micrographs were captured at 10 kV acceleration voltage, with working distances of 20 mm (image overview, Figure 10A) and 4.5 mm (Figure 10B), respectively.

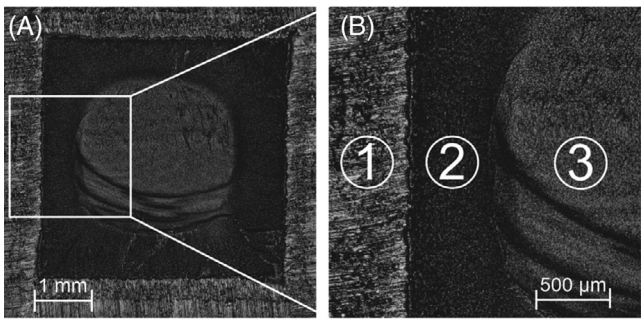

FIGURE 4 Grayscale laser scanning microscopy reflective images of the fracture surface at 85% of expected time to failure of AGUV exposed to Arkopal, (A) overview, (B) detailed view exhibiting (1) notch area A_n, (2) crack region, (3) cryo-fractured area.

4.2.2 | X-ray micro computed tomography scan (CT)

CT measurements were conducted employing a custom-built X-ray micro-CT system that incorporated essential components allowing for a detailed analysis. The system comprised a manipulator, a 225 kV X-ray tube supplied by X-Ray WorX GmbH (Garbsen, Germany), and a flat panel detector with dimensions of 2048 × 2048 pixels from Perkin Elmer, Inc (Waltham, MA, USA). To facilitate measurements, the FNCT specimen under examination was positioned on a rotatable table, situated in-between the X-ray tube and the detector (as depicted in Figure 6). Throughout the process, the object underwent a complete 360-degree rotation within its horizontal plane, with radiographed images taken at evenly spaced rotation increments. The accumulation of 3000 projection images enabled the generation of a volume-based dataset using the cone-beam algorithm formulated by Feldkamp.[37]

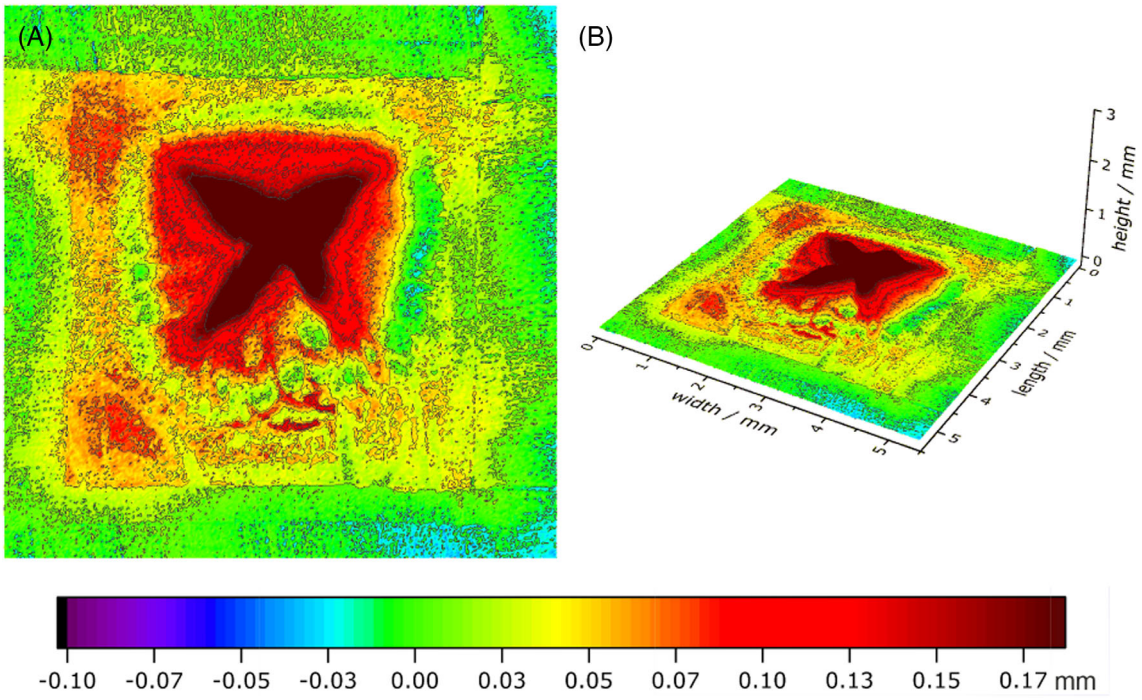

FIGURE 5 Exemplary 3D laser scanning microscopy height profiles; (A) top view, (B) side view.

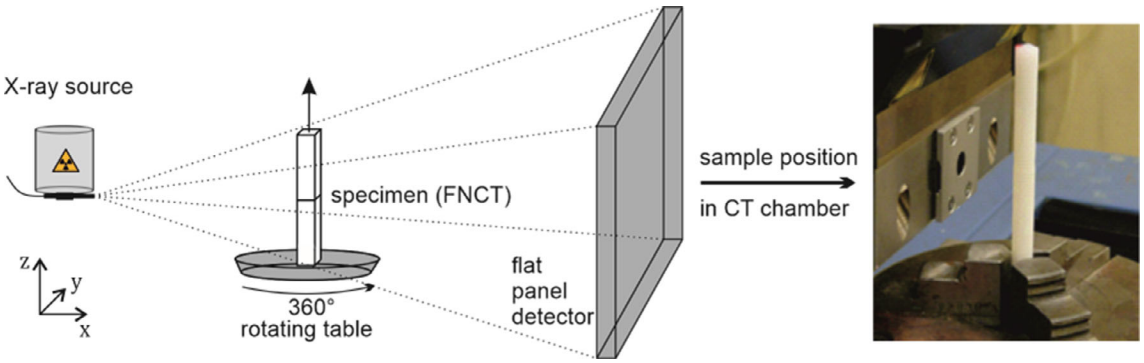

FIGURE 6 Schematic depiction of X-ray micro computed tomography scan (CT) measurement and test piece position in front of the X-ray tube during the CT measurement.

A single voxel, constituting a three-dimensional volume element within the dataset, corresponded to dimensions of 5.4 × 5.4 × 5.4 mm^3. These voxels carried information about the X-ray attenuation coefficient within their volume, as indicated by corresponding gray values. Given the sample's relatively low attenuation, a conservative energy setting of 60 kV was selected for all measurements. Notably, each projection image was exposed for a duration of 6 seconds.

The three-dimensional representations reconstructed from the CT data underwent thorough evaluation using VGStudio 3.0, a software developed by Volume Graphics GmbH (Heidelberg, Germany) explicitly designed for visualizing and analyzing of industrial CT data. It is worth to mention that no modifications were required for the FNCT specimens to facilitate CT measurements, as the device conveniently accommodated the entire specimen. This favorable circumstance enabled the utilization of a single specimen for all measurements. Accordingly, a singular specimen underwent partial damage via FNCT, followed by CT scanning, and subsequently underwent further exposure within the FNCT device. Consequently, this streamlined approach enabled the investigation of four distinct stages of damage on a single specimen.

In contrast to the initial approach employing gray-scale images from LSM, the evaluation of crack-growth did not involve averaging of crack lengths derived from a normalized area representation of the partially damaged

fracture surface. Instead, a more direct route was adopted in which individual crack lengths were determined directly using the suite of tools available within the 3D visualization software. This led to the derivation of crack length assessments by averaging the single measurements, 25 in each edge direction, resulting in a total of 100 measurements of crack lengths, as formalized by Equation (6).

5 | RESULTS AND DISCUSSION

In our previous study,[3] significant disparities in the calculated apparent crack propagation rates were observed (see Figure 9). It was evident that the differences in crack growth rates could not be solely attributed to the distinct capabilities of the various imaging techniques. Instead, this discrepancy could be better explained by the assumption of a length of the antecedent craze zone increasing as the crack grew. Such an assumption is substantiated by the fact that during an FNCT experiment, mechanical stress promotes the formation of crazes to a significantly greater extent in comparison to the initial phases of crazing and crack propagation. This effect enlarges both the craze zone and the adjoining region of plastic deformation.[4,38]

Considering the overall crack length and the corresponding craze zone, it is possible to establish a linear correlation between the two by applying fracture mechanical considerations. This relationship is derived from the Irwin model (Equation 2 in Section 2) and the mathematical interpretation of the Dugdale plastic zone model (illustrated in Figure 1) by Rice.[23] The expression for this relationship, which is formulated in terms of the craze zone length (as represented by Equation 4), is based on the premise that at the point of crack propagation, craze stress (σ_c) and fracture stress (σ_B) must be equivalent ($\sigma_c = \sigma_B$). This assumption is founded on the idea that every fibril within the craze zone experiences a form of tensile test in the course of craze-crack propagation, analogous to the behavior of the entire HDPE material during a tensile test. More detailed insight into this concept can be found in Figure 10. By combining Equations (2) and (4), the following linear correlation emerges:

$$s_{craze} = \frac{\pi}{8}\frac{\left[\sigma_B(\pi c)^{1/2}\right]^2}{\sigma_c^2} \Leftrightarrow s_{craze} = \frac{\pi}{8}\frac{\sigma_B^2}{\sigma_c^2}\pi c \overset{\sigma_B=\sigma_c}{\Leftrightarrow} s_{craze} = \frac{\pi^2}{8}c \tag{8}$$

with s_{craze}: craze zone length and c: crack length.

Hence, there is a linear correlation according to:

$$s_{craze} \propto c. \tag{9}$$

Because $\frac{\pi^2}{8} > 1$, the craze zone length s_{craze} is always longer than the crack length c.

This correlation establishes a linear relationship between the craze zone length s_{craze} and the length of the crack c (Figure 7). Consequently, it confirms the assumption that during crack growth, the craze zone does not propagate with a constant length; instead, it grows in tandem with the increase in crack length. Simultaneously, the undamaged residual fracture path p_{urf} is decreasing. p_{urf} is oriented within the plane and direction of crack growth and simply represents the region not yet damaged by crack or by craze. Due to the symmetry of the FNCT specimen's cross section, it is formally defined as the distance between the end of the current craze zone and the center of the specimen. Therefore, upon the FNCT specimen's complete failure, p_{urf} is zero by definition. Due to the interrelation between crack length and length of the craze zone, specimens or components with a specific crack length have experienced already a substantially

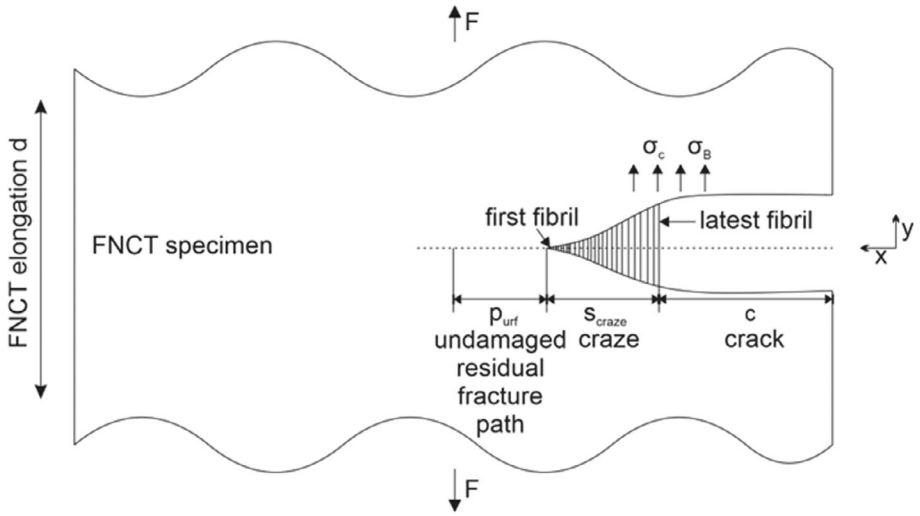

FIGURE 7 Craze zone and crack of a specimen schematically representing the status during full notch creep test.

further damage by crazing. In later stages of the crack propagation, despite a substantial extent of the craze zone, the craze fibrils might exhibit lesser elongations due to the restricted internal deformation above and below the plane of the crack, being required to facilitate the further opening of the crack. This leads to a greater tendency for these fibrils to undergo partial relaxation and appear undamaged when subjected to destructive imaging techniques after dissection of specimen. This is a known feature of residual fibrils on fracture surfaces.[8,9,39] Destructive imaging techniques tend to identify portions of the actual craze zone as undamaged, initially. On the contrary, nondestructive imaging methods distinguish between damaged and undamaged matrix material based on effective density (optical density for X-ray and velocity of ultrasound for SAM). This distinction between craze and crack becomes less straightforward, as both exhibit reduced density. Consequently, this distinction can introduce discrepancies in crack lengths and is particularly evident as an offset in the time-dependent curves deduced from optical analysis (Figure 9).

However, the deviations observed between the destructive (i) LM/LSM and nondestructive (ii) SAM/CT methods in Schilling et al. (2018)[3] are more accentuated with increased lengths of the crack and craze zones. As a result, the apparent crack propagation rates derived from both (i) and (ii) methods diverge significantly, as indicated in Figure 9 and Schilling et al. (2018).[3] Additionally, CT images (based on differences in optical density between HDPE and air) imply the existence of a substantial craze zone (as can be seen in Figure 12).

To visualize the above assumptions and the correlation between the length of crack and craze (as expressed in Equation 8), an analysis was conducted to correlate experimentally measured crack lengths c with derived values for craze lengths s_{craze}, as well as undamaged residual fracture path p_{urf} (as depicted in Figure 8).

Within this analysis, crack lengths in the region of linear crack growth (Figure 8) refer to the values of linear regression of LSM crack length data (Figure 9, dashed line). Consequently, craze lengths were determined based

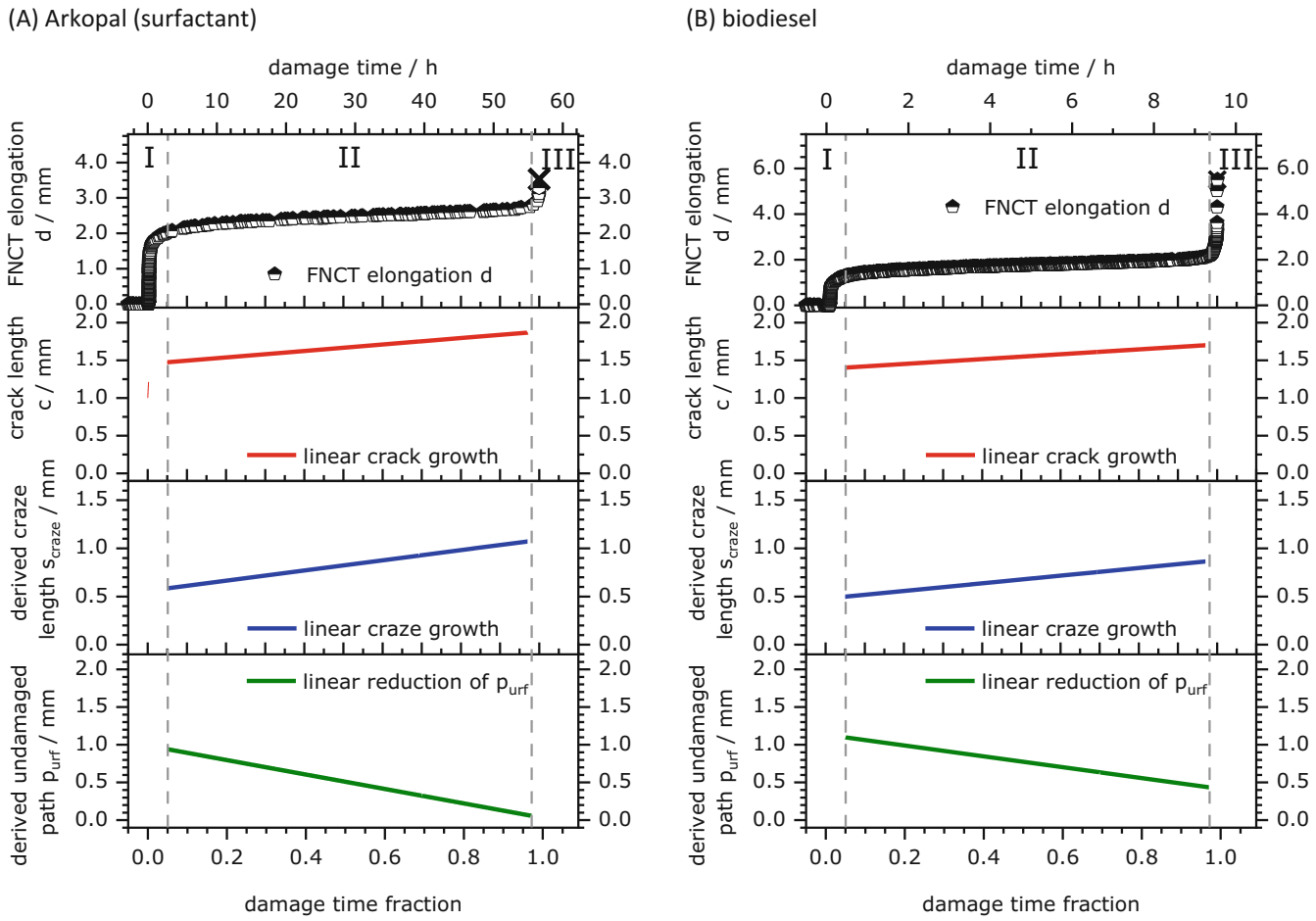

FIGURE 8 Comparison of measured full notch creep test elongation d and linear regression of crack length increase (crack length c including notch from laser scanning microscopy grayscale reflective images) with derived craze lengths s_{craze} and undamaged residual fracture paths p_{urf}.

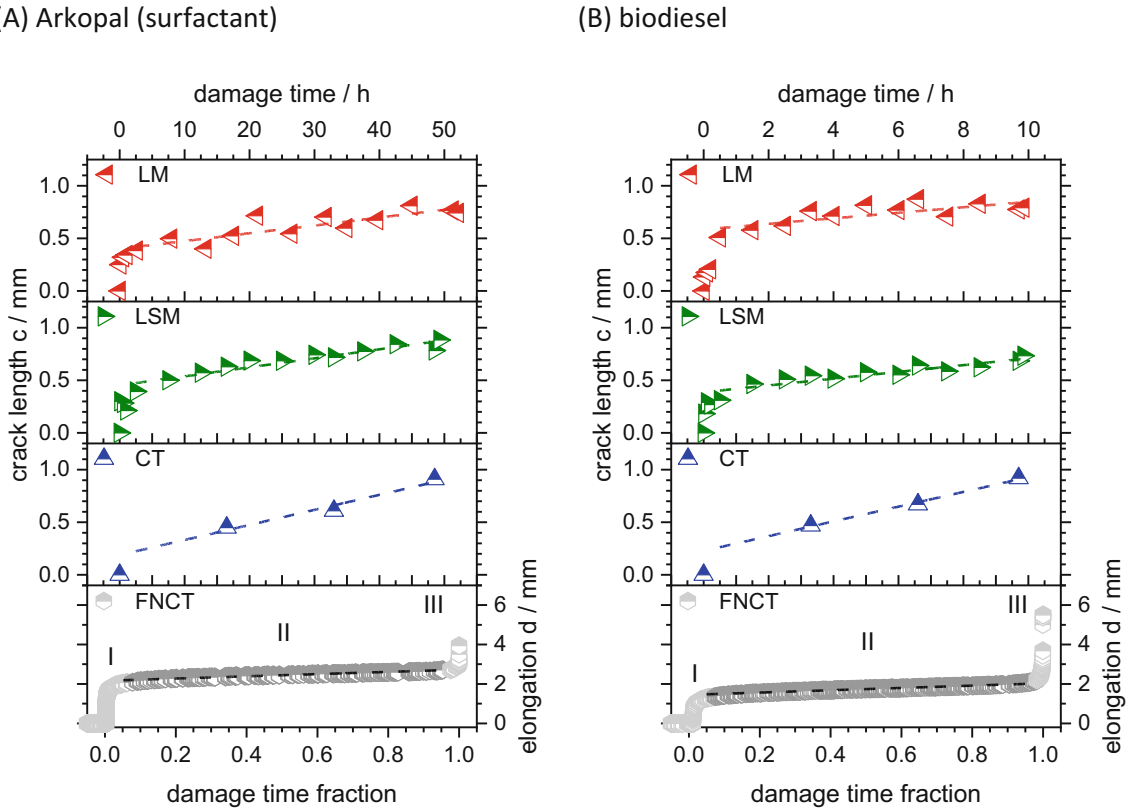

FIGURE 9 Average crack lengths and apparent crack growth rates determined from light microscopy, laser scanning microscopy, and X-ray micro computed tomography scan (in Arkopal[3]—LM: 12.2 μm/h, LSM: 13.5 μm/h and CT: 22.3 μm/h, in biodiesel[31]—LM: 26.3 μm/h, LSM: 32.3 μm/h and CT: 70.2 μm/h) compared to full notch creep test elongation data.

on linear crack growth data from LSM and Equation 8 for the subsequent comparison.

Notably, these craze lengths (Figure 8) were established from crack length data (Figure 9) without including the notches since crazes emerge immediately after notching due to the initiation of crack propagation under constant load. Furthermore, the undamaged residual fracture path (p_{urf}) was derived by subtracting the current crack length (excluding the notch) as well as the craze length from the initial p_{urf} value. This analysis specifically pertains to the scenario of a single crack propagating from the edge to the center of an FNCT specimen, as depicted in Figures 7 and 11. Consequently, the initial p_{urf} value (as per Equation 10) is 2 mm:

$$p_{\mathrm{urf,\ start}} = \frac{1}{2}\,\text{FNCT specimen width} - \text{notch depth} = \frac{1}{2}\,6\,\text{mm} - 1\,\text{mm}. \quad (10)$$

The initial region I of the test encompasses approximately 5% of t_f^* and represents the period in which the applied force takes effect. During this period, initial crazes form, and crack growth initiates. The lengths of both the craze and crack zones experience significant expansion. In region II, characterized by consistent crack growth, both crack and craze lengths linearly increase. In parallel, the undamaged residual fracture path (p_{urf}) progressively decreases (Figure 8).

In Arkopal, the undamaged residual fracture path reaches nearly zero at around 97% t_f^*. As a consequence, the specimen is predominantly damaged by either cracks or crazes at this point. The ultimate failure of the specimen, occurring in region III, becomes an inevitability. The abrupt nonlinear spike in elongation observed in region III is due to the considerable high level of true mechanical stress resulting from the diminished ligament area ($p_{urf} \to 0$). It is essential to acknowledge that the true stress necessary to induce the final failure (the transition from region II to region III) is related to the yield strength of the polymer, as evaluated through conventional tensile testing. The true stress is calculated from the constant force related to the actual residual cross-sectional area A_{ud} (cf. Figure 3) as measured on fracture surfaces (similar to Equation 5). Once the true stress aligns with the yield strength value, the craze-crack mechanism evolves into deformation by shear. This shift results in the appearance of an elongated central

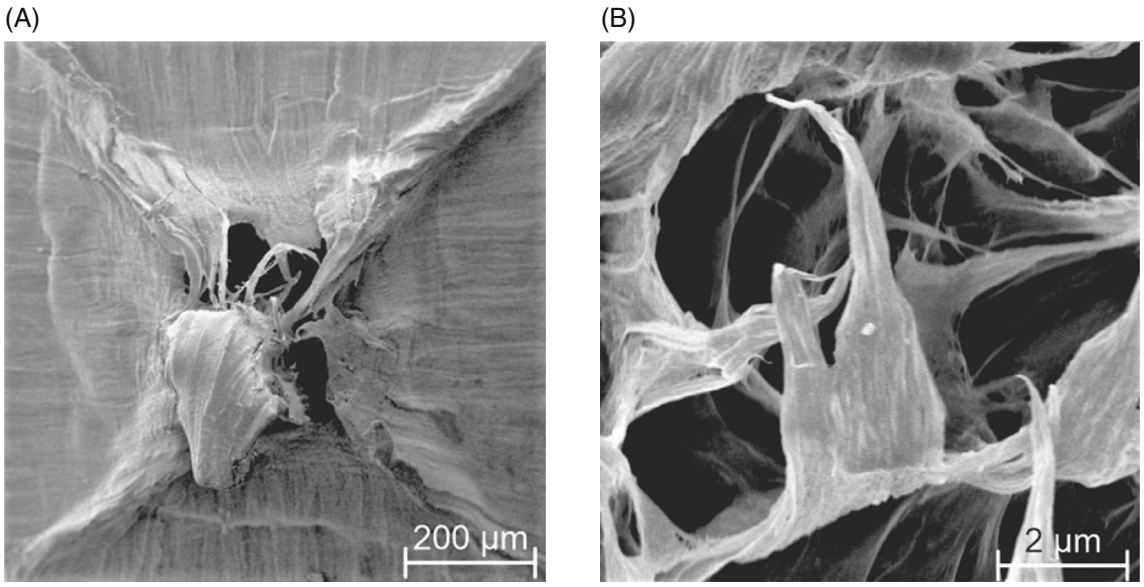

FIGURE 10 Scanning electron microscopy images of fibrils in different length scales (full notch creep test, Arkopal, 50°C, $\sigma_n = 9$ MPa).

ligament, a well-known feature in this context (Figure 10A and[8]).

A notable feature of this phenomenon is the striking scalability of ductile effects on the fracture surface across macroscopic and microscopic length scales. This underpins the assumption that each fibril undergoes a form of tensile test similar to the behavior of the entire bulk material in the course of the craze-crack mechanism. This similarity is evident across multiple length scales in terms of the typical fracture surface features.[40] These features manifest during gradual crack growth and relate to both the overall appearance of individual fibrils within the craze-crack mechanism and the entirety of the fracture surface during the final stages of the test, symbolizing ductile failure akin to fracture surfaces resulting from tensile tests. This phenomenon is exemplified in Figure 10, where the central ligament on a scale of a few hundred micrometers is juxtaposed with a single fibril measuring about one micrometer. Both instances exhibit ductile failure, albeit on different scales. This similarity confirms the foundational assumption ($\sigma_c = \sigma_B$) upon which the theoretical considerations (Equation 8) are based.

In Arkopal, the yield strength (≈24 to 25 MPa[29]) is reached by the true stress when the material is already significantly damaged by either craze or crack ($p_{urf} \approx 0$). The presence of sorptive liquids, that is, liquids that are absorbed by HDPE to a certain extent, like biodiesel introduces a reduction in yield strength (≈21 to 22 MPa for AGUV) due to the effects of swelling and plasticization.[41,42] As a result, the true stress that is necessary to induce the transition from craze-crack propagation to ductile shear deformation is lowered by biodiesel in comparison to the aqueous surfactant solution. Consequently, this transition takes place even if the fracture path is not entirely damaged, yet ($p_{urf} > 0$, Figure 8). This leads to the coexistence of cracked (1), crazed (2), and undamaged (3) regions in the fracture zone of FNCT specimens exposed to sorptive fluids at the juncture of the transition from craze-crack propagation to deformation by shear. Intriguingly, the FNCT fracture surfaces directly reflect these conditions at the point of transition, as evidenced in Figure 11 in which these regions are marked, with the case of sorptive biodiesel presented in Figure 11B. In contrast, the fracture surface of the specimen exposed to Arkopal exhibits a large central ligament due to ductile shear deformation, even though there was no undamaged residual fracture path left when ductile failure started ($p_{urf} \approx 0$). Consequently, this final ductile failure occurred on a zone that was already crazed before.

It should be noted at this point that the state of sorption of biodiesel is mainly determined by diffusion during the 10-h conditioning period as part of the standard FNCT procedure and therefore far from saturation and equilibrium with respect to the bulk of the specimen, which is finally reached after >1000 h. In this context, one must consider that the discussion is primarily aimed at the qualitative description of the different behavior in sorptive and non-sorptive media related to the occurrence of craze zone and crack. Furthermore, the remarkable yellowish coloration of the surface restricted to the fracture zone in Figure 11B (not visible in the notch area!) points very likely to a drastically different sorption

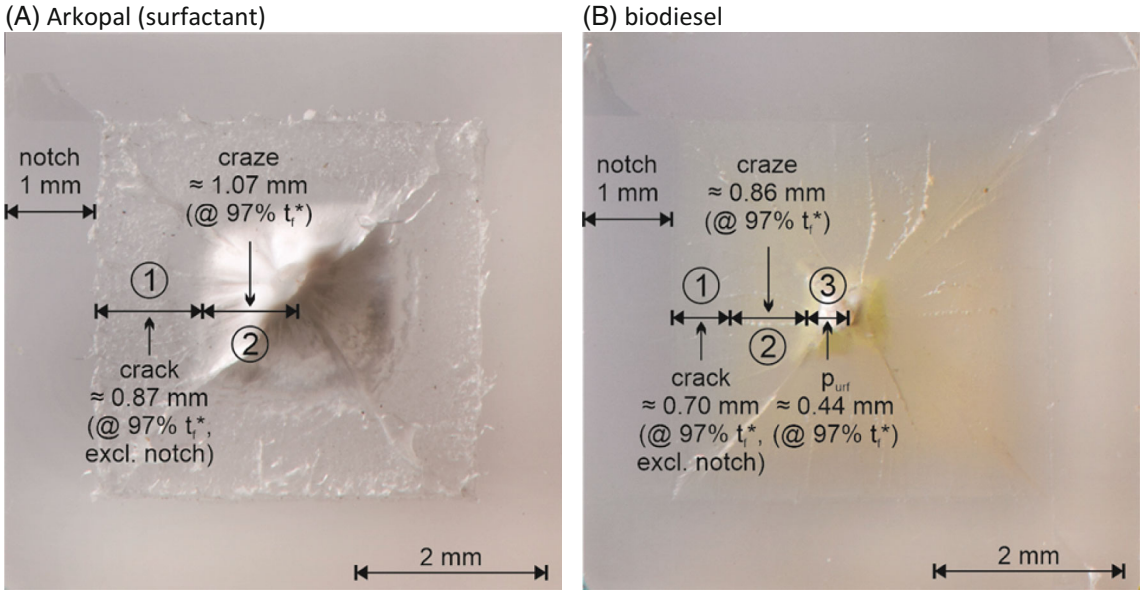

FIGURE 11 Correlations of crack and craze lengths c and s_{craze}, respectively as well as undamaged residual fracture paths p_{urf} with typical features of a fracture surface from full notch creep test, exemplary shown for AGUV in Arkopal (surfactant) and biodiesel.

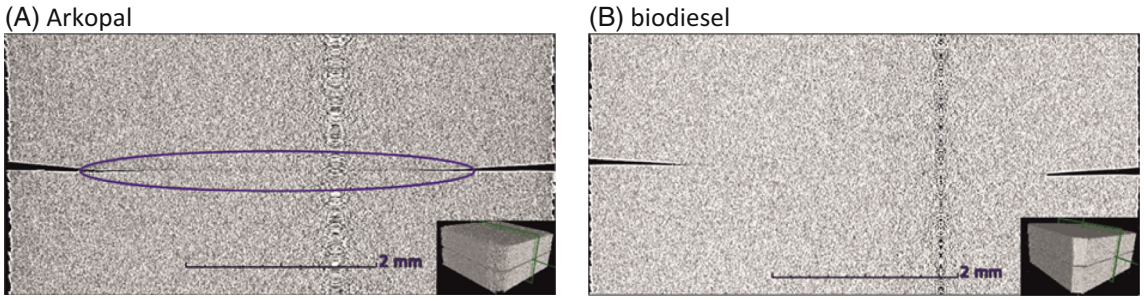

FIGURE 12 X-ray micro computed tomography scan side view images of AGUV full notch creep test specimens loaded for 97% t_f* in a) Arkopal[3,38] and b) biodiesel.[38]

behavior of this fracture zone compared to the bulk. Therefore, the consideration of different concentration levels and the related time-dependencies exceeds the scope of this work and requires further extensive studies.

Based on the side view CT image,[3] it can be inferred that a craze zone has already spread throughout the entire cross section of the FNCT specimen loaded for 97% t_f* in Arkopal, as can be seen in the marked zone in Figure 12A. However, in the case of the FNCT specimen exposed under load to biodiesel, a residual undamaged fracture path is still present after 97% t_f*, as evidenced by $p_{urf}>0$ (Figure 11) and therefore, the craze zone does not span the entire residual cross section of the specimen, yet (Figure 12B). At this point, it has to be noticed that the CT images alone may not be entirely conclusive as the voids in the crazed porous regions might contain the sorptive medium biodiesel, leading to reduced X-ray contrast between HDPE and the liquid. This can potentially obscure the clear identification of crazed regions present.

Nevertheless, the coherent presence of the continuous craze zone over the whole cross section of the FNCT specimen visible in the CT image shown in Figure 12 is concordant with the calculated craze zone length and the fracture surface depicted in Figure 11A.

The observed distinct characteristics discernible on the final fracture surface are directly attributable to the conditions of the different regions at the onset of shear deformation (i.e., transition from region II to III at approximately 97% t_f*). Regions fully cracked at this point in time display macroscopically brittle failure, as evidenced by the lawn-like surface features derived from cracked fibrils. On the other hand, those regions on the resulting fracture surface with craze damage exhibit elongated fibrils and elevated characteristics (such as plateaus

and pillow-like features as shown in Figure 11A,B) when subjected to high stresses exceeding the yield strength of the bulk HDPE material in region III. Meanwhile, the undamaged bulk material (p_{urf}) becomes drawn into even higher (central) ligaments (as depicted in Figure 11B). The differences between these regions are readily distinguishable.

Consequently, this analysis of the fracture surface unveils that even regions previously subjected to crazing undergo shear deformation upon reaching the corresponding stress threshold. This observation can be interpreted as macroscopically ductile fracture behavior, which becomes a part of the central ligament (particularly as in Figure 11A). This might be surprising, as a macroscopic ductile portion on an FNCT fracture surface could intuitively be attributed to failure stemming from pure shear deformation in entirely undamaged HDPE regions. In contrast, the presence of cracked, crazed, and undamaged regions, represented by their respective lengths, is evident on the fracture surfaces (as shown in Figure 11B). The plateau structures, akin to pillow-like features observed on fracture surfaces resulting from FNCT in sorptive fluids, emerge from elongated and saturated fibrils that were initially part of the crazed region before final ductile failure. Despite this pre-damage by the craze-crack mechanism, these structures eventually fail due to shear deformation. This observation aligns with the time-dependent optical monitoring of crack opening displacement under similar conditions by Thuy et al.,[5] highlighting the decisive impact of the final stages of the FNCT experiment on specimen failure and the ensuing fracture surface.

6 | CONCLUSION

Utilizing the established methodology of the FNCT and employing a comprehensive analysis of the fracture surface through various microscopic imaging methods, described in a previous study,[3] the time-dependent progression of SCG or rather ESC in HDPE, both based on a craze-crack mechanism, was thoroughly investigated. In particular, a high-performance blow-molding grade of HDPE for container applications was investigated in the standard detergent Arkopal as surface active agent in aqueous solution and also in biodiesel as sorptive environmental medium at the standard conditions specified for blow-molding materials,[7] that is, 9.0 MPa at 50°C.

By analysis of a series of partially damaged specimens, the determination of crack propagation rates was possible. As noticed earlier,[3] the different imaging techniques lead to slightly deviating propagation rates which were ascribed to differences regarding the respective distinction between craze zone and crack. Furthermore, it was assumed that the length of the anteceding craze zone increases with increasing crack length to completely explain the observed deviations. The latter was confirmed in this work by theoretical considerations based on fracture mechanics and a linear relation of craze length and crack length was derived (Equations 8 and 9). The overall phenomenon was verified by similar results for a second system: HDPE in biodiesel.

Comparing the results obtained from the different imaging techniques, those obtained from LSM seem to be the most reliable and were used to calculate the actual lengths of craze, crack, and undamaged regions which could be clearly assigned to the respective regions of actual fracture surfaces. This demonstrates again the informative value of a detailed fracture surface analysis with respect to the progression of crack propagation and the underlying mechanisms. In this context, it could be shown that an already pre-damaged craze zone not always ends in a propagating crack but might also fail due to ductile deformation when the respective conditions (actual stress) are reached. This confirms the conjecture of a continuous craze zone found in X-ray micro computed tomography data.[3] Furthermore, this is supported by the optical monitoring of the time-dependent crack opening displacement (COD) of an FNCT specimen by Thuy et al.[5]

Additionally, it could be demonstrated that the influence of plasticization by the sorptive medium leads to a premature transition from crack propagation to ductile failure due to a significant reduction of the yield stress, corroborating a direct relation between this transition and the yield stress.

ACKNOWLEDGMENTS

The authors appreciate the help of O. Schwarze and N. Schmidt for preparation of the specimens and C. Weimann for the SEM micrographs. Furthermore, we would like to thank I. Alig and H. Oehler of Fraunhofer LBF for valuable discussions in the framework of the joint research project. Open Access funding enabled and organized by Projekt DEAL.

FUNDING INFORMATION

The authors are grateful for financial support of AiF (Arbeitsgemeinschaft industrieller Forschungsvereinigungen) within the program for sponsorship by Industrial Joint Research (IGF) of the German Federal Ministry of Economic Affairs and Climate Action (BMWK) based on an enactment of the German Parliament, IGF grant number 18606 N.

DATA AVAILABILITY STATEMENT

The raw/processed data required to reproduce these findings cannot be shared at this time as the data also form part of an ongoing study.

ORCID

Markus Schilling https://orcid.org/0000-0002-7094-5371
Ute Niebergall https://orcid.org/0000-0002-4970-7627
Niklas Marschall https://orcid.org/0009-0001-0315-3964
Dietmar Meinel https://orcid.org/0000-0003-1015-441X
Martin Böhning https://orcid.org/0000-0001-9753-345X

REFERENCES

1. Wright DC. *Environmental Stress Cracking of Plastics*. Rapra Techology Ltd.; 1996.
2. Almomani A, Mourad A-HI, Deveci S, Wee J-W, Choi B-H. Recent advances in slow crack growth modeling of polyethylene materials. *Mater Design*. 2023;227:111720. doi:10.1016/j.matdes.2023.111720
3. Schilling M, Niebergall U, Alig I, et al. Crack propagation in HDPE induced by environmental stress cracking (ESC) analyzed by several imaging techniques. *Polym Test*. 2018;70:544-555. doi:10.1016/j.polymertesting.2018.08.014
4. Brown N, Lu X. A fundamental theory for slow crack growth in polyethylene. *Polymer*. 1995;36:543-548. doi:10.1016/0032-3861(95)91563-M
5. Thuy M, Niebergall U, Oehler H, Alig I, Böhning M. Damaging effect of admixtures used in crop protection products on high density polyethylene packaging material. *Polym Test*. 2022;114:107672. doi:10.1016/j.polymertesting.2022.107672
6. Thuy M, Niebergall U, Oehler H, Alig I, Böhning M. Evaluation of the damaging effect of crop protection formulations on high density polyethylene using the full notch creep test. *Polymer*. 2021;228:123853. doi:10.1016/j.polymer.2021.123853
7. International, A. Plastics—Determination of environmental stress cracking (ESC) of polyethylene—Full-notch creep test (FNCT), ISO 16770:2019.
8. Schilling M, Niebergall U, Böhning M. Full notch creep test (FNCT) of HDPE—characterization and differentiation of brittle and ductile fracture behavior during environmental stress cracking (ESC). *Polym Test*. 2017;64:156-166. doi:10.1016/j.polymertesting.2017.09.043
9. Schilling M, Niebergall U, Marschall N, Alig I, Böhning M. A phenomenological criterion for an optical assessment of HDPE fracture surfaces obtained from FNCT. *Polym Test*. 2021;94:107002. doi:10.1016/j.polymertesting.2020.107002
10. Fleissner M. Experience with a full notch creep test in determining the stress crack performance of polyethylenes. *Polym Eng Sci*. 1998;38:330-340. doi:10.1002/pen.10194
11. Ayyer R, Hiltner A, Baer E. Effect of an environmental stress cracking agent on the mechanism of fatigue and creep in polyethylene. *J Mater Sci*. 2008;43:6238-6253. doi:10.1007/s10853-008-2926-1
12. Schilling M, Böhning M, Oehler H, Alig I, Niebergall U. Environmental stress cracking of polyethylene high density (HDPE) induced by liquid media—validation and verification of the full-notch creep test (FNCT). *Mat Sci Eng Tec*. 2017;48:846-854. doi:10.1002/mawe.201700065
13. Griffith AA. The phenomena of rupture and flow in solids. *Philos Trans R Soc*. 1921;221:163-198. doi:10.1098/rsta.1921.0006
14. Irwin GR. Analysis of stresses and strains near the end of a crack traversing a plate. *J Appl Mech Tran ASME*. 1957;24:351-369.
15. Berry JP. Determination of fracture surface energies by cleavage technique. *J Appl Phys*. 1963;34:62-68. doi:10.1063/1.1729091
16. Orowan E. Surface energy and surface tension in solids and liquids. *Proc R Soc Lon, Ser A: Math Phys Sci*. 1970;316:473-491. doi:10.1098/rspa.1970.0091
17. Macmillan NH, Kelly A. Relationship between ideal tensile-strength and surface-energy. *Mat Sci Eng*. 1972;10:139-143. doi:10.1016/0025-5416(72)90078-x
18. Andrews EH. Fracture mechanics approach to corrosion stress cracking in plastics. *Proceedings of the Conference on the Physical Basis of Yield and Fracture*. Institute of Physics & The Physical Society London; 1966:127.
19. Kambour RP. A review of crazing and fracture in thermoplastics. *J pol Sci Macrom Rev*. 1973;7:1-154.
20. Kambour RP. Structure and properties of crazes in polycarbonate and other glassy polymers. *Polymer*. 1964;5:143-155. doi:10.1016/0032-3861(64)90128-4
21. Kambour RP. Mechanism of fracture in glassy polymers. 3. Direct observation of craze ahead of propagating crack in poly(methyl methacrylate) and polystyrene. *J Polym Sci, Part A-2: Polym Phys*. 1966;4:349. doi:10.1002/pol.1966.160040305
22. Dugdale DS. Yielding of steel sheets containing slits. *J Mech Phys Solids*. 1960;8:100-104. doi:10.1016/0022-5096(60)90013-2
23. Rice JR. *Fracture—an Advanced Treatise*. Academic Press; 1968.
24. Rice JR. A path independent integral and approximate analysis of strain concentration by notches and cracks. *J Appl Mech*. 1968;35:379-386. doi:10.1115/1.3601206
25. Chan MKV, Williams JG. J-integral studies of crack initiation of a tough high-density polyethylene. *Int J Fract*. 1983;23:145-159. doi:10.1016/0032-3861(83)90139-8
26. Mai YW, Cotterell B. On the essential work of ductile fracture in polymers. *Int J Fract*. 1986;32:105-125. doi:10.1007/bf00019787
27. Wu JS, Mai YW. The essential fracture work concept for toughness measurement of ductile polymers. *Polym Eng Sci*. 1996;36:2275-2288. doi:10.1002/pen.10626
28. Williams JG, Rink M. The standardisation of the EWF test. *Eng Fract Mech*. 2007;74:1009-1017. doi:10.1016/j.engfracmech.2006.12.017
29. Technical data sheet—Lupolen 4261 AG UV 60005, polyethylene, high density, Basell Polyolefine GmbH, Frankfurt, Germany, Release date: 26th of July 2004. Also available at https://www.lyondellbasell.com
30. International, A. Automotive fuels—Fatty acid methyl esters (FAME) for diesel engines—Requirements and test methods; German version DIN EN 14214:2003.
31. Schilling M. Environmental Stress Cracking (ESC) and Slow Crack Growth (SCG) of HDPE induced by external fluids., Darmstadt 2020, Technische Universität Darmstadt (Dissertation). 10.25534/tuprints-00011544
32. International, A. Plastics—Compression moulding of test specimens of thermoplastic materials (ISO 293:2004), German version DIN EN ISO 293:2005.

33. International, A. Plastics—Polyethylene (PE) moulding and extrusion materials—Part 2: preparation of test specimens and determination of properties (ISO 17855-2:2016), German version DIN EN ISO 17855-2:2016.
34. International, A. Packaging—Transport packaging for dangerous goods—Plastics compatibility testing for packaging and IBCs (ISO 13274:2013 + Cor. 1:2014), German version DIN EN ISO 13274:2013 + AC:2014.
35. International, A. Plastics—Ultra-high-molecular-weight polyethylene (PE-UHMW) moulding and extrusion materials—Part 2: preparation of test specimens and determination of properties (ISO 11542-2:1998 + Cor. 1:2007), German version DIN EN ISO 11542-2:1998 + AC:2008.
36. Renka RJ, Cline AK. A triangle-based c-1 interpolation method. *Rocky Mt J Math*. 1984;14:223-237. doi:10.1216/rmj-1984-14-1-223
37. Feldkamp LA, Davis LC, Kress JW. Practical cone-beam algorithm. *J Opt Soc Am A*. 1984;1(6):612-619. doi:10.1364/josaa.1.000612
38. Menges G. Das Verhalten von Kunststoffen unter Dehnung. *Kunststoffe*. 1973;63:95-100.
39. Deblieck R, Gerets B, Boerakker M, Caelers H, Wilbers A, Boonen T. Relation between life time, failure stress and craze microstructure in polyethylene as evidenced by fracture surface texture analysis after an accelerated full-notch creep test. *Polymer*. 2019;176:264-273. doi:10.1016/j.polymer.2019.04.033
40. Thuy M, Spyrantis A, Böhning M, Niebergall U, Maaß R. Spatially resolved roughness exponent in polymer fracture. *Phys Rev Mater*. 2022;6:L090601. doi:10.1103/PhysRevMaterials.6.L090601
41. Validierung und Weiterentwicklung des "Full Notch Creep Tests" zur Bewertung von Kunststoffen für Gefahrgutbehälter, final report of AiF/IGF/FGK joint project 18606N elaborated by BAM, Berlin and Fraunhofer LBF, Darmstadt from 1st July 2015 to 30th August 2018, IGF Schlussbericht. 2018.
42. Böhning M, Niebergall U, Zanotto M, Wachtendorf V. Impact of biodiesel sorption on tensile properties of HDPE for container applications. *Polym Test*. 2016;50:315-324. doi:10.1016/j.polymertesting.2016.01.025s

How to cite this article: Schilling M, Niebergall U, Marschall N, Meinel D, Böhning M. Relation of craze to crack length during slow crack growth phenomena in high-density polyethylene. *Polym Eng Sci*. 2024;64(6):2387-2403. doi:10.1002/pen.26698